Final Report

Cover Page

Report Number:	DOEPBL19722
DOE Award Number:	DE-SC0019722
Sponsoring Program Office:	DOE Office of Science
Name and Address of Recipient:	Particle Beam Lasers, Inc. 18925 Dearborn Street Northridge, CA 91324-2807
Project Title:	HTS Solenoid for Neutron Scattering
Principal Investigator:	Robert J. Weggel
Team Members:	Robert J. Weggel, Ramesh Gupta, Ronald Scanlan, Erich Willen, Stephen Kahn, James Kolonko, Delbert Larson, William Sampson, Shresht Joshi, Raymond Ceruti and Stephan Plate

Acknowledgement: This material is based upon work supported by the U.S. Department of Energy, Office of Science, Office of Basic Energy Sciences, under Award Number DE-SC0019722.

Project Summary / Abstract

Company Name and Address: Particle Beam Lasers, Inc.
18925 Dearborn Street
Northridge, CA 91324-2807

Principal Investigator: Robert J. Weggel

Project Title: HTS Solenoid for Neutron Scattering

US neutron scattering facilities are currently limited to ~16 T, which is insufficient to study the structure and dynamics of ultra-high magnetic field states of quantum matter and materials processed in high magnetic fields. To remedy this, proposals were requested for very high field magnets suitable for neutron-scattering applications.

Particle Beam Lasers, Inc. (PBL) and the Superconducting Magnet Division of Brookhaven National Laboratory (BNL) responded with a proposal to advance magnet technology for neutron-scattering experiments by capitalizing upon their expertise and equipment, some of which was developed during several SBIR/STTR collaborations, including one that designed, built and tested a solenoid that generated nearly 16 T, a world record in 2013 for a magnet exclusively of high temperature superconductor (HTS). BNL also has built and tested an HTS magnet for superconducting magnetic energy storage, and is building a 25 T solenoid for Axion research.

Proposed are magnet designs of a revolutionary geometry that provides generous viewing access radially, axially, and circumferentially. The designs exploit outboard coils to magnetically attract inboard coils so strongly as to overpower the attractive force from coils on the opposite side of the magnet midplane. These inner coils therefore need no midplane-straddling structure for mechanical support. Support of the outboard coils is at a radius so large as to block little of the circumference of the midplane viewing port.

Phase I benefited from the participation of BNL scientists involved in neutron-scattering experiments to generate preliminary designs of 25 T magnets that satisfy their challenging requirements. A major computational task was to optimize the magnet design to reduce cost in materials and fabrication and to limit the strain on conductors. An experimental task was to utilize HTS tape on hand to wind coils of conical shape and to test them at 77 K. Phase II would extend the theoretical and experimental studies of Phase I to a Proof-of-Principle demonstration magnet.

Commercial Applications and Other Benefits: Many consider neutron scattering to be the most valuable of all tools for investigating matter, employing many thousands of researchers. Their research is of great commercial as well as intellectual value, justifying the expenditure of billions of dollars on neutron sources, detectors and magnets. The R&D proposed by this SBIR/STTR was to further the technology to design, fabricate and test proof-of-principle and prototype magnets, and thereby to increase even further the value of neutron scattering.

Key Words: Magnet, solenoid, high-temperature superconductor, HTS, neutron scattering

Summary for Members of Congress: This SBIR/STTR was to develop the technology for a 25 T magnet for neutron scattering, which many consider to be the most valuable—commercially as well as academically—of all tools for investigating matter.

Identification and Significance of the Problem or Opportunity, and Technical Approach

Neutron scattering experiments would benefit from magnets with fields at least 50% more intense than the ~17 T presently available from conventional low-temperature superconductors (LTS). A high temperature superconductor (HTS) such as ReBCO, operating at ~4 K as a **high field** superconductor, is essential, because LTS falls far short of the needed combination of critical field and critical current density.

To advance magnet technology for neutron-scattering experiments, Particle Beam Lasers, Inc. (PBL) and the Superconducting Magnet Division (SMD) of Brookhaven National Laboratory (BNL) have capitalized upon their expertise and equipment, some of which was developed during SBIR/STTR collaborations, including ones that designed, built and tested the two HTS solenoids of Fig. 1, designed to be capable of nesting to generate a field to reach the desired range.

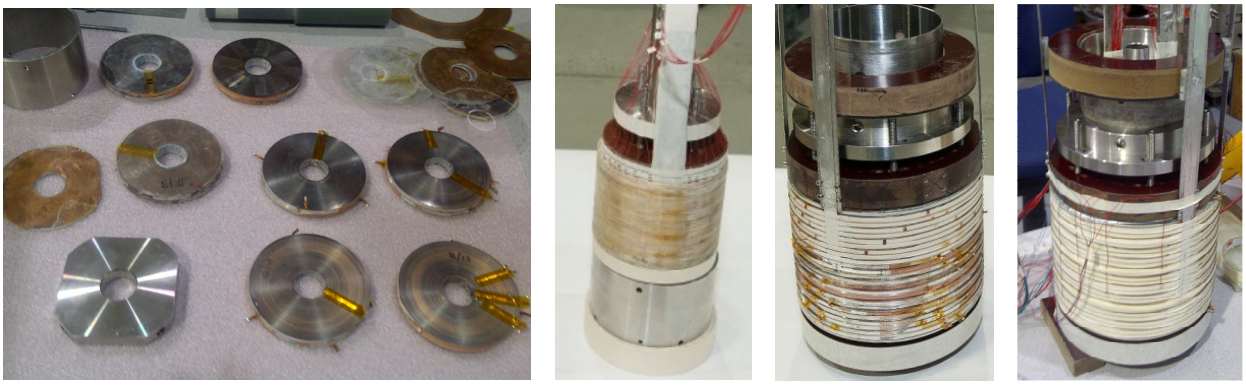

Fig. 1a-d.: High field HTS solenoids designed, built and tested by PBL/BNL collaborations. Left: 25-mm bore pancake coils for insert magnet. Left-center: Solenoid that generated 16 T. Right-center: Solenoid with 12 double-pancakes of 100 mm bore. Right: Nested set.

The inner of these two solenoids, of 25-mm i.d. and 91-mm o.d., operated at a current density greater than 500 A/mm^2 and generated nearly 16 T, a world record in 2013 for a magnet exclusively of HTS. The outer solenoid had respective inner and outer diameters of 100 mm and 163 mm. A half-length version generated more than 6 T (maximum ambient field = 9.2 T). Full length, its designed contribution is 10 T; nested, the pair of solenoids might be capable of 25 T or more. These solenoids employed metallic (stainless steel) insulation; the technology led to further R&D at BNL on HTS magnets. BNL also has tested magnets with conventional insulation and no insulation.

Another valuable legacy of previous PBL/BNL collaborations is the advanced system of Fig. 2, to detect incipient magnet quenches and shut down the magnet to protect it from burnout. Such a system is essential to successful magnet operation.

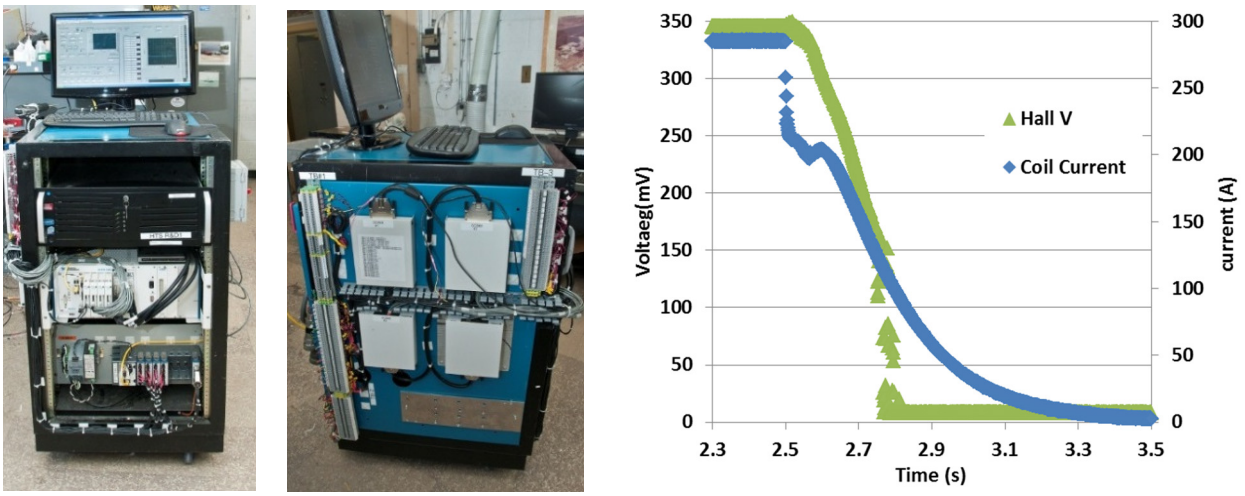

Fig. 2a-c. Quench-detection and magnet-protection system developed during PBL/BNL SBIR/STTR collaborations. Left & center: Hardware (32 channels, 1 kV). Right: Time dependence of magnet's current—and also central field, as measured by Hall voltage—during rapid shutdown. The very rapid drop in current from 285 A to 230 A is from inductive commutation of current to copper discs between the magnet's double pancakes of conductor.

The major experimental accomplishment in Phase I was to utilize conductor on hand at BNL to wind conical coils of ReBCO tape and to test them at 77 K. The major analytical accomplishment was to generate preliminary designs of 25-T magnets with many nested solenoids, using HTS in all coils that see a field higher than 14 T. Valuable in this endeavor was input from Drs. Igor Zaliznyak and John Tranquada of BNL, and Dr. Roy I. Cutler of ORNL, all experts in the field of neutron scattering experiments.

Design requirements for a high field magnet for neutron scattering

High magnetic field is an important tool for tuning the state of matter, creating new states and quantum phases, and changing the fundamental properties of materials. Magnetic fields can modify transport properties of conductors, correlations in magnetic insulators, and the way conduction electrons interact with atomic moments in magnetic metals. Neutron-scattering techniques provide a powerful tool for studying these atomic, molecular and microscopic properties and correlations in condensed matter systems. The importance of developing high magnetic field environments for such studies has therefore been widely appreciated, e.g., in the National Research Council of the National Academy of Sciences report, "High Magnetic Field Science and Its Application in the United States: Status and Future Directions".[1] Workshops by the ORNL Neutron Science Directorate[2-4] discussed advances in high magnetic field science and practical routes for building high-field magnets for neutron scattering to enable the new science that neutron-scattering measurements in high magnetic fields can provide. A recent Workshop[4] focused on the new opportunities provided by the progress in the commercial development of high-temperature superconductor technology.

Low-temperature superconductor (LTS) magnets for neutron-scattering measurements can reach only ~17 T. To reach 26 T, the dedicated beam line EXED at the Helmholtz Zentrum, Berlin (HZB)[5,6] augmented the field from the superconducting outer coils with 11 teslas from a resistive insert consuming 4.4 MW, at a capital cost of $30 M for the resistive magnet, power supply and cooling system, and also operating costs orders of magnitude greater than for an all-superconducting system.

The magnetic field is horizontal, with a viewing angle of only 30°. The geometry severely limits neutron spectroscopic studies, which require rotation of the sample with respect to the detector array and the incident beam in order to explore its reciprocal space. HTS coils should be able to deliver magnetic fields as intense as 25 T.[4] A 25 T split-coil, vertical-field magnet could be similar in usability and versatility to the LTS systems that are currently the mainstay of neutron scattering studies. Ideally, the magnet would be experiment-friendly, with large viewing ports (~90° to 180° circumferentially and flaring ±5° to ±15° in breadth) and compact and portable between different neutron spectrometers, rather than requiring a dedicated beam line.

Magnet design and requirements

The main requirement for a neutron or X-ray-scattering magnet is a large solid angle for the passage of incident and scattered beams, unobscured by the magnet coils or their support structure. Especially for time-of-flight (TOF) neutron spectroscopy, the viewing ports should be as free as possible of material, to avoid spurious TOF background features from neutrons scattering in, for example, thin-walled aluminum cylinders separating the members of a split-coil pair.[7-9]

Two basic magnet geometries are used to position the coils out of incident and scattered beam paths in neutron-scattering magnets: (i) vertical-field (VF), split-coil, and (ii) horizontal-field, conical-bore. The latter optionally may split the coil to accommodate the incident beam and/or the top-loading sample environments. The former is used in most high field LTS magnets for neutron scattering; the HZB uses the latter. The horizontal field geometry also is used in some scattering experiments that require the field direction to be paraxial with the incident beam, or to rotate in the horizontal scattering plane. These include some experiments using reflectometry or small-angle neutron scattering (SANS), or that require the field to be quasi-parallel with the momentum transfer vector, which usually is in the horizontal scattering plane. The LTS magnets used for such measurements typically have horizontal-field, conical-bore geometry with an opening up to 90° (±45°) that can be positioned either along, or perpendicular to, the incident beam. For the latter, the coil usually is split to accommodate the incident beam as well as the top-loading sample environments. Horizontal-field magnets typically have fields lower than vertical-field systems, usually no more than 9 T; the recent 17 T SANS magnet[10] has only limited acceptance.

Preferred is the vertical-field, split-coil geometry, which is compatible with the sample rotation techniques for broad surveys of reciprocal space. Furthermore, stray fields at the side of magnets typically are only half that at the same distance along the axis and easier to shield or to mitigate using compensation coils. Additionally, the geometry more easily accommodates ^{3}He and dilution-refrigeration inserts, pressure cells, and high-temperature inserts, providing opportunities for neutron studies under multiple extreme thermodynamic conditions. For these reasons, the recommendation of the Ultra-High Field Magnets for X-Ray and Neutron Scattering Using High Temperature Superconductors Workshop was to concentrate on developing magnets with the vertical-field, split-coil geometry.[4]

Table 1 presents magnet parameters specified in an ORNL solicitation for a magnet of 25 T.

Table I: Illustrative Specs of 25 Tesla Magnet for Diffraction Measurements

Maximum field	25 teslas
Field homogeneity:	< 1.4% over cylinder of 15 mm diameter and length
Stray field (at maximum field)	≤ 0.1 T @ 2 m; ≤ 0.01T @ 4 m
Minimum open bore diameter	40 mm
Minimum coil split height	17 mm
Vertical opening	–5° to +5°, flaring from ±7.5 mm, the ends of the sample
Horizontal opening	4 openings, each ±30°), flaring from ±7.5 mm, the sample radius

Anticipated Public Benefits

A publication[11] by the Institute of Physics states, "Neutron scattering is routinely used in modern science to understand material properties on the atomic scale. Originally developed as a tool for physics, the method has led to advances in many areas of science, from clean energy and the environment, pharmaceuticals and healthcare, through to nanotechnology, materials engineering, fundamental physics and IT. …

"Neutron scattering is used in many different scientific fields. Neutrons can be used to study the dynamics of chemical reactions at interfaces for chemical and biochemical engineering, in food science, drug synthesis and healthcare. Neutrons can probe deep into solid objects such as turbine blades, gas pipelines and welds to give microscopic insight into the strains and stresses that affect the operational lifetimes of crucial engineering components. Neutron studies of nano-particles, low-dimensional systems and magnetism are used for the development of next-generation computer and IT technology, data storage, sensors and superconducting materials. Neutron scattering is a delicate and non-destructive measurement technique, making it ideal for use in heritage science. …

"Neutron scattering can be used to address the global challenges facing society, and to make developments that have immediate or long-term economic impact."

Many consider neutron scattering to be the most valuable of all tools for investigating matter of all sorts, employing thousands of researchers, as evidenced by organizations such as the Neutron Scattering Society of America and the European Neutron Scattering Association. Their research is of extreme commercial as well as intellectual value, justifying the expenditure of billions of dollars on neutron sources and detectors, including magnets such as those from HTS-110, a division of the SCOTT Group.

As with nuclear magnetic resonance, sensitivity and resolution improve **very** greatly with increased magnetic field intensity. The R&D of this SBIR/STTR, to develop the technology to design, fabricate and test proof-of principle and prototype magnets, has the potential to broaden and deepen greatly the value of neutron scattering, carrying it into a new regime of utility. Developing the technology for such magnets is vital for their success, and therefore amply justifies the investment.

May contain trade secrets or commercial or financial information that is privileged or confidential and exempt from public disclosure. Such proprietary information is highlighted.

PBL/BNL experience in high field HTS solenoid development

PBL and BNL have extensive experience in high field HTS solenoid technology, collaborating on several Phase I and Phase II SBIRs supported by the Office of High Energy Physics. The solenoid of Fig. 1b, consisting of seven double pancakes of 25 mm i.d., generated 16 T, a record field at that time for an all-HTS solenoid. The solenoid of Fig. 1d, with twelve double pancakes of 100 mm bore, designed as an outsert for the inner HTS solenoid, generated, at only half length (Fig. 1c), 6.4 T on-axis and 9.2 T maximum. Both solenoids used insulation of stainless steel.

In addition, as described in the Related Research section below, Dr. Gupta and his BNL team have designed, constructed, and tested many other large high-field HTS magnets, including a solenoid for superconducting magnetic energy storage (SMES). The team led a project to fabricate a 25 T solenoid of 100 mm bore for the Institute for Basic Science (IBS).

PBL consulted distinguished members of the user community as part of the effort. PBL's relationship with scientists at BNL and ORNL provided valuable input to the "Proof-of-Principle" demonstration magnet that we are proposing to build in Phase II and on the requirements for the high field magnet for the Neutron scattering magnet we hope to help build beyond the Phase II.

Geometry of Illustrative Neutron-Scattering Magnets of Three Designs

Figures 3 and 4 reveal the geometry of three illustrative designs for magnets to generate 25 T for neutron scattering experiments. Figure 3 presents views from above a quadrant of the upper half of each magnet; Figure 4 presents views from below.

Figures 3a and 4a show a geometry in which coils bear on a platen near the magnet midplane, which in turn bears on pie wedges to withstand the enormous Lorentz force with which magnet halves attract each other across the magnet midplane. Bridging the circumferential spans between the wedges is a platen postulated to have the strength and stiffness of stainless steel. Stiffer alternatives could reduce these deformations; candidates to consider are tungsten, molybdenum, or steels stiffened by large percentages of titanium diboride. Circumferentially between pie wedges are ports that allow scattered neutrons to reach detectors without traversing material other than cryostat walls.

Figures 3b and 4b show a design in which the platen is much further from the magnet midplane, thereby appropriating volume that is much less efficient for generating magnetic field. Supporting the platen are rings interpolated radially between selected inboard coils to carry the magnetic force with which the outboard coils are attracted toward the magnet midplane by the other coils. The inboard coils need no mechanical support, because they are attracted more strongly upward by the outboard coils than downward by the coils across the midplane.

Figures 3c and 4c show a design that threads the load-bearing rings between radial gaps between outboard coils rather than inboard ones, appropriating volume that is of even lower quality for generating field. The rings, now in axial tension rather than compression, hang from a thick outboard platen cantilevered from a comparably-thick ring radially beyond all of the magnets. Because the cross-midplane support is now at such a large radius, it need block only a small fraction of the available circumference.

May contain trade secrets or commercial or financial information that is privileged or confidential and exempt from public disclosure. Such proprietary information is highlighted.

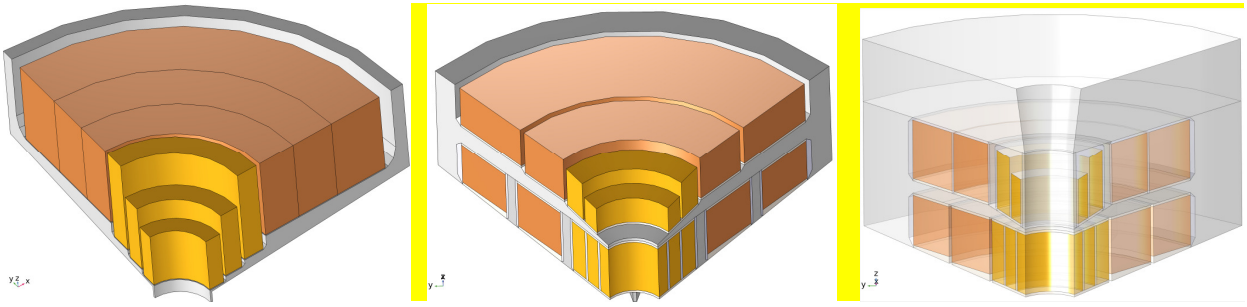

Fig. 3a-c. Views from above a quadrant of the upper half of illustrative magnets to meet the specs of Table I. Gold-colored is ReBCO tape; copper-colored is low-temperature superconductor (LTS); grey is support-structure material, typically stainless steel. Left: Coils supported by platen near magnet midplane; platen sits on midplane pie wedges. Center: Outboard coils rest on platen supported by rings that sit on midplane pie wedges. Right: Platen held by rings extending downward from a thick outboard cantilever.

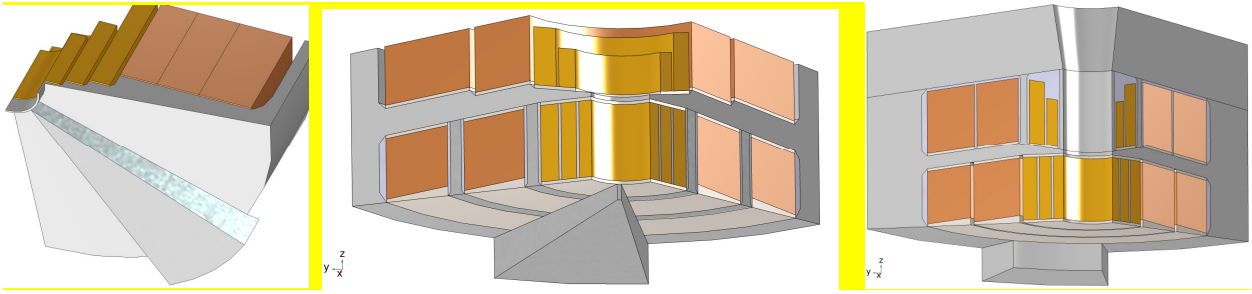

Fig. 4a-c. Views from below a quadrant of the upper half of the illustrative magnets of Fig. 3. Below each quadrant is a pie wedge (blunt-nosed in 4c), flaring axially by ~5° and circumferentially by ~30°, that bears the cross-midplane force of attraction between the coils above and below the magnet midplane

Figure 5a-c shows illustrative sets of pie wedges associated with an upper half-magnet. In 5a and 5b, the circumferential extent of each half-port is 30°+10 mm. In 5c, with its two quadrant pie wedges not diametrically opposite each other, but centered on ±75°, the outlet port has a circumferential extent of ±60°.

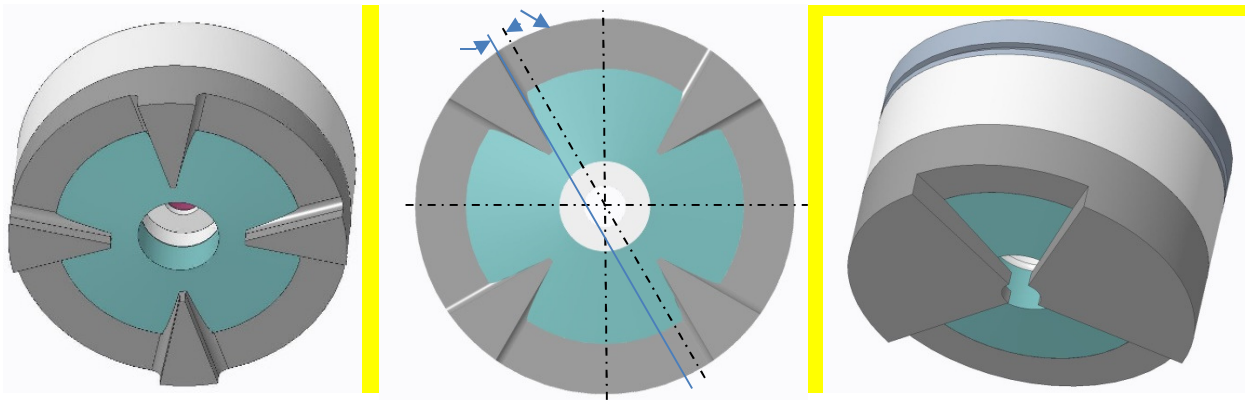

Fig. 5a-c. Underside views of top half of magnets, to reveal shape and orientation of pie wedges that support cross-midplane Lorentz loads.

May contain trade secrets or commercial or financial information that is privileged or confidential and exempt from public disclosure. Such proprietary information is highlighted.

Geometry with Coil Support very near Midplane of Magnet

The magnet of Fig. 3a/4a generates the field distribution shown in Fig. 6. Its maximum field is 29.16 T; that seen by the Nb_3Sn is 14 T. The total magnetic energy of the magnet is 1.42 MJ. The axial magnetic force of attraction between the two magnet halves is 3.29 MN.

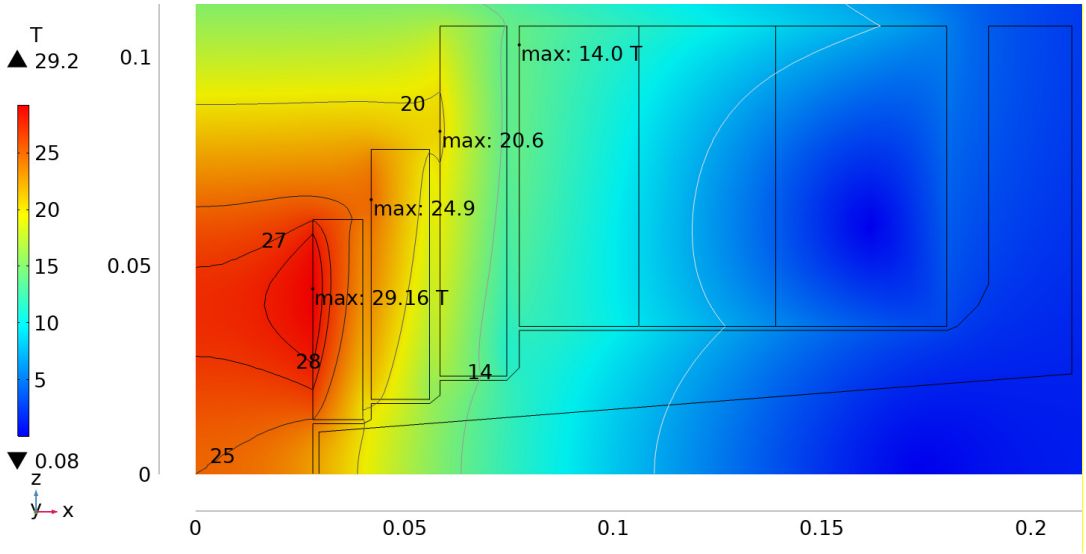

Fig. 6. Field magnitude of magnet of Fig. 3a/4a. The maximum ambient field is 29.2 T; that seen by the Nb_3Sn is 14 T. Tesla contours are 7, 14, 20, 25, 27 and 28. The total magnetic energy of the magnet is 1.42 MJ. The axial magnetic force of attraction between the two magnet halves is 3.29 MN.

Figures 7 and 8 plot the von Mises stress and first principal strain in this illustrative magnet. Table II lists selected parameters of the magnet, including an estimate of cost with which to compare the cost of two subsequent designs.

May contain trade secrets or commercial or financial information that is privileged or confidential and exempt from public disclosure. Such proprietary information is highlighted.

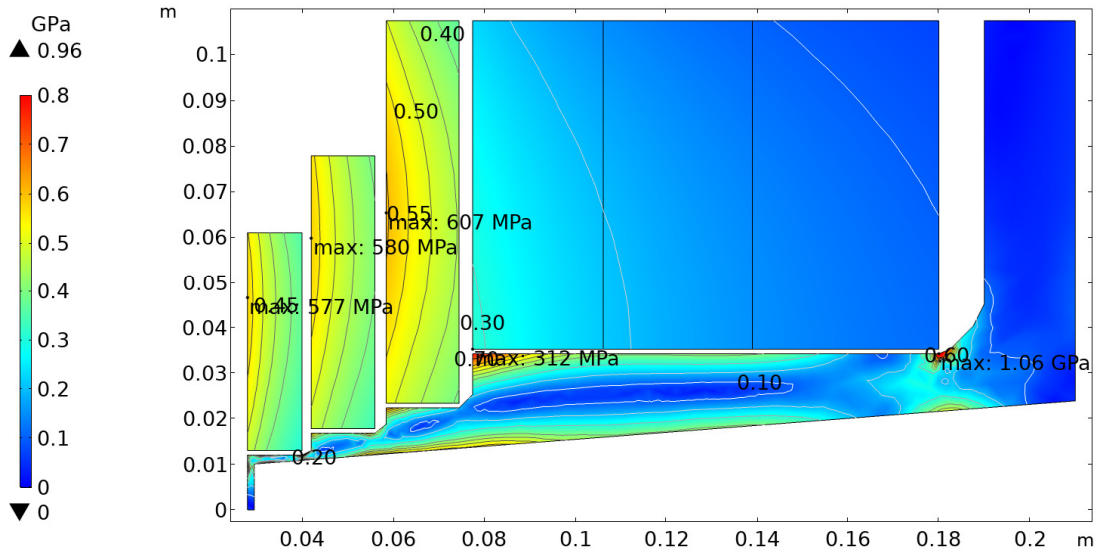

Fig. 7. Von Mises stress σ_{vM} in magnet of Figs. 5&6. The maximum von Mises stress in each of the three ReBCO coils is approximately 600 MPa, the maximum recommended for the conductor; σ_{vM} in the Nb_3Sn reaches 312 MPa. In the support material the maximum stress, 1.06 GPa, probably is sufficiently localized to be acceptable.

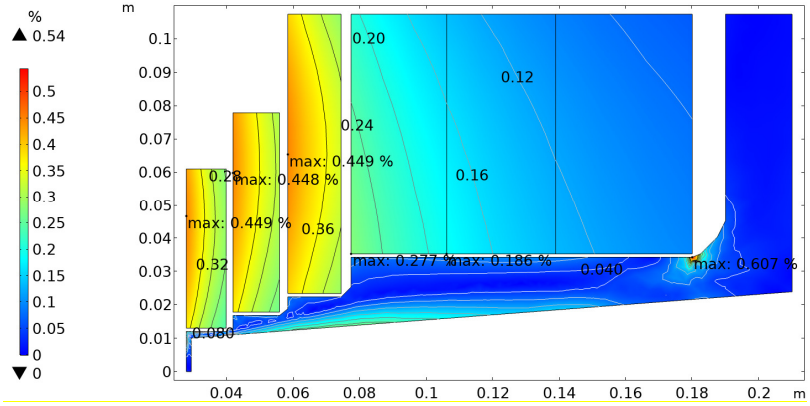

Fig. 8. First principal strain ε_1 in magnet of Figs. 6 & 7. The maximum strain in each of the three ReBCO coils is 0.45%, the maximum recommended for the conductor; ε_1 in the Nb_3Sn reaches 0.277%. In the support material the maximum strain, 0.61%, probably is sufficiently localized to be acceptable.

May contain trade secrets or commercial or financial information that is privileged or confidential and exempt from public disclosure. Such proprietary information is highlighted.

Table II: Parameters of Illustrative Magnet with Coil Support near Magnet Midplane

Inboard-platen design: Cost ratio defined to be 100%

Parameter	units	Spec	Magnet	YBCO #1	YBCO #2	YBCO #3	Nb_3Sn	Structure
Minimum bore	mm	40.0	56.0					
Minimum split	mm	17.0	19.9					
Min. midplane taper angle	degrees	±5.0	±5.0					
Axial taper angle	degrees		23.1					
Current density	A/mm²		515	515	450	445	260	
B_0, cubic discretization	T	25.0	25.00	3.99	3.98	4.63	12.40	
$\Delta B/B_0$ 15 mm diam. & length	%	1.40	1.39					
Maximum ambient field	T		29.2	29.2	24.9	20.6	14.0	
Magnetic energy	kJ		1422					
Max. r j B hoop stress	MPa		519	496	491	519	272	
Bonded-coil von Mises stress	MPa		607	577	580	607	312	1060
Bonded-coil hoop strain	%		0.449	0.449	0.448	0.449	0.277	0.607
Downward Lorentz force, Fz	kN		3287	-33	30	462	2828	
Material	- - -			YBCO	YBCO	YBCO	Nb_3Sn	Steel
Conductor requirement	cm³			246	517	1123	11957	8723
Normalized unit cost	- - -			1	1	1	0.2	0.01
Normalized cost of material	- -		4365	246	517	1123	2391	87
Percentage of total cost	%		100.0%	5.6%	11.8%	25.7%	54.8%	2.0%
$\Delta B_0/\Delta\$$	~ T/$		25.0	70.7	33.6	18.0	22.6	

Technical Objectives: Concept of Revolutionary, Open-Midplane Design of Magnet

The revolutionary designs whose development this SBIR/STTR advanced employ magnetic attraction instead of mechanical support for the inner solenoids of a magnet with multiple nested split-solenoids—i.e., solenoids with a midplane gap, as in a Helmholtz pair. Coils that are outboard (i.e., relatively far from the magnet midplane) magnetically attract inboard coils so strongly as to overpower the attractive force from coils on the opposite side of the magnet midplane. These inner coils therefore need no midplane-straddling structure for mechanical support. Support for the outboard coils straddles the midplane, but only through pie wedges confined to circumferential regions that are at least ±30° from the axis of the viewing port. Inspiration for the design was the "open-midplane dipole" design[11,12] proposed nearly two decades ago by Ramesh Gupta and pioneered by a collaboration of PBL and BNL.[13]

To increase viewing port angles and magnet efficiency, coils ideally have a cross section that is not a rectangle but a parallelogram, with its inboard edge paralleling the flare angle of the magnet's midplane viewing port. Wherever the field is too intense for low-temperature superconductors, the conductor is ReBCO tape, assumed 12 mm wide, wound into pancakes that are dished slightly into a very blunt cone, like a nearly flat cone spring. Figure 9 illustrates this key component to improve magnet efficiency and field homogeneity. A task completed by this SBIR was the winding of such coils and testing them at 77 K.

May contain trade secrets or commercial or financial information that is privileged or confidential and exempt from public disclosure. Such proprietary information is highlighted.

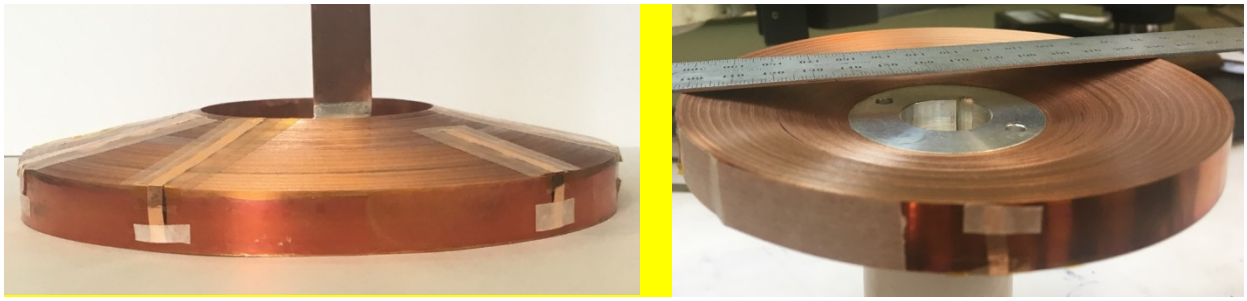

Fig. 9. Conical coil of 315 turns (88 m) of ReBCO tape 12 mm wide and 0.12 mm thick, wound by the BNL Superconducting Magnet Division. I.D. = 51 mm; O.D. = 127 mm; cone angle = 15°; cone height = 10 mm.

Design with Magnetic Support of Inboard Coils, Intercoil Platen Support from Below

Figures 10 and 11 plot the magnetic field intensity throughout the magnet. Coil dimensions attempt to minimize the use of expensive HTS, substituting Nb_3Sn or NbTi wherever the ambient field is not too intense.

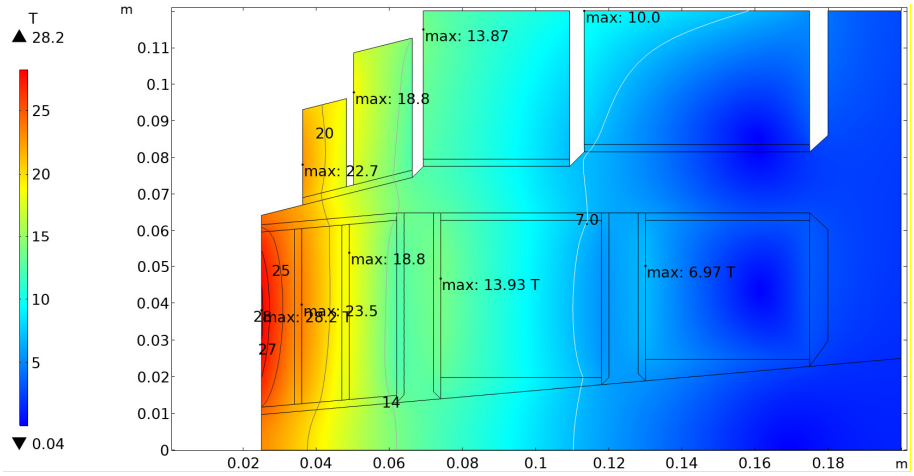

Fig. 10. Field magnitude B of magnet of Figs. 3b/4b. The midplane cone angle is ±5°; axial access is ±18°. B_{max} in the ReBCO tape is 28.2 T; selected contours suggest where Nb_3Sn or NbTi suffices instead of HTS: 14 T for Nb_3Sn and 7 T for NbTi. The magnetic energy, U_m, is 1.29 MJ.

May contain trade secrets or commercial or financial information that is privileged or confidential and exempt from public disclosure. Such proprietary information is highlighted.

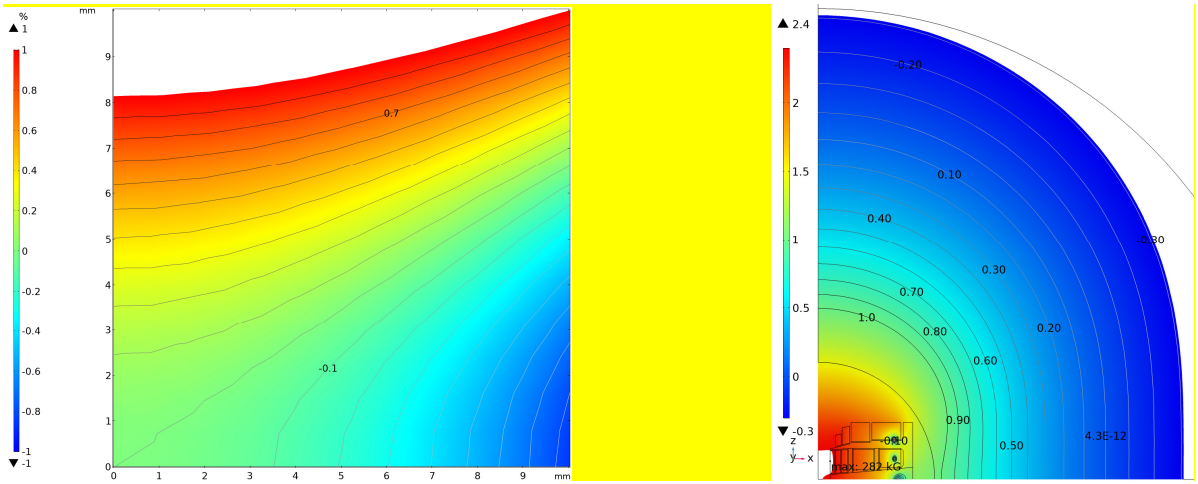

Fig. 11a&b. Field homogeneity and fringe field. Left: The peak-to-peak field inhomogeneity is 1.39% over a cylinder of 7.5 mm radius and half-length. Right: log10|*B*[kG]|. The successive kG contours are [$10^{-0.3}$=0.5, 0.64, 0.8, 1.0, 1.25, 1.6, 2, 2.5, 3.2, 4.0, 5.0, 6.4, 8.0, 10]. On-axis, the blue-to-white border ($10^{-0.3} \approx 0.5$ kG) nearly reaches the black arc, $r = 1$ m; extrapolating $B \sim r^{-3}$ predicts a field approximately one sixteenth the allowed 0.1 T (1 kG) at 2 m.

Figure 12 plots $|F_z|$, the absolute value of the density of the axial component of Lorentz force, facilitating comparison of the upward and downward forces by displaying equal magnitudes as equal colors. Throughout the white band within each coil $|F_z|$ is less than 0.2 N/mm^3. Above the band, forces are downwards, toward the magnet midplane; below the band, they are upwards. The net force, in kN, on each of the five successive inboard coils is 0.04, 4.1, 9.5, 24 and 0.8—every one upwards, as intended. The downward force on successive outboard coils is 86, 309, 869 and 2090 kN, a net downward force of 3.32 MN.

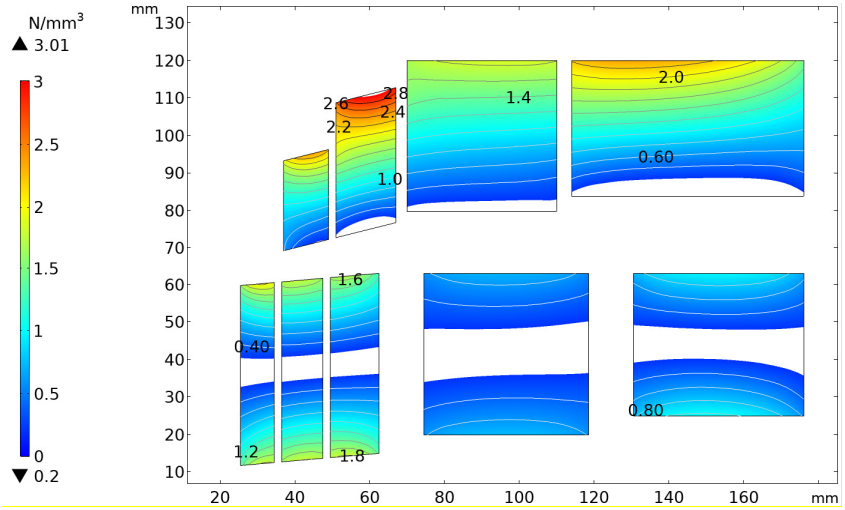

Fig. 12. Absolute value of axial Lorentz force density in magnet of Fig. 10. Magnetic attraction from outboard coils attracts inboard coils upward, overpowering the downward attraction from coils on the opposite side of the midplane. Within the white band, $|F_z| < 0.2$ N/mm^3. Axially outboard of the band, F_z is toward the magnet midplane; axially inboard, it is away. The net force on each inboard coil is away from the midplane.

May contain trade secrets or commercial or financial information that is privileged or confidential and exempt from public disclosure. Such proprietary information is highlighted.

Figures 13&14 plot the vertical displacement of coils and platen. The coils are postulated to be orthotropic, with circumferential, axial and radial Young's moduli of [150, 120, 30] for ReBCO and [100, 20, 20] for both Nb_3Sn and NbTi. The support structure is isotropic, postulated to have the Young's modulus of molybdenum: 312 GPa. With such a stiff support material, the maximum displacement is only 0.28 mm in the platen and 0.35 mm in the conductor.

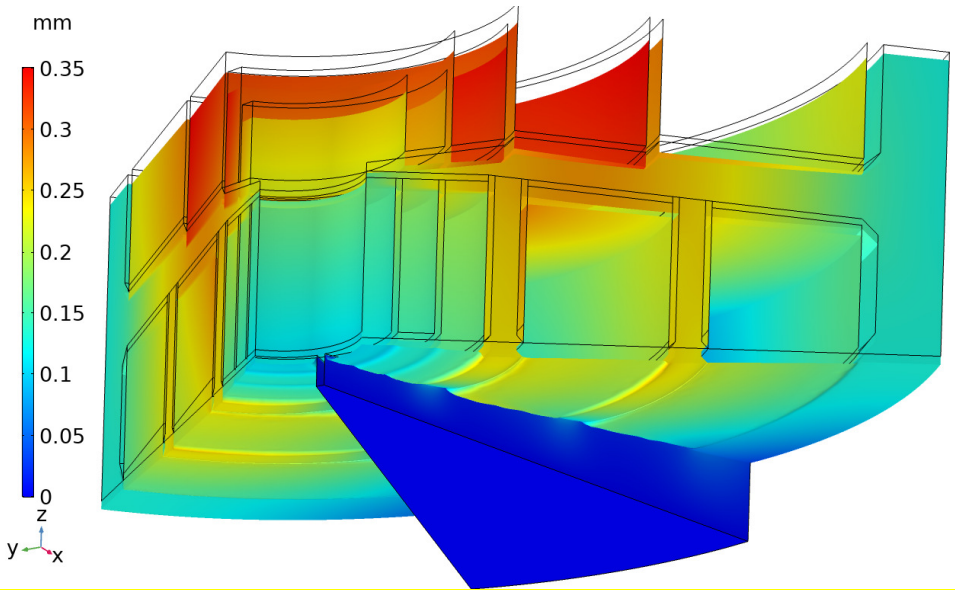

Fig, 13. Axial displacements δ_z, magnified twentyfold.

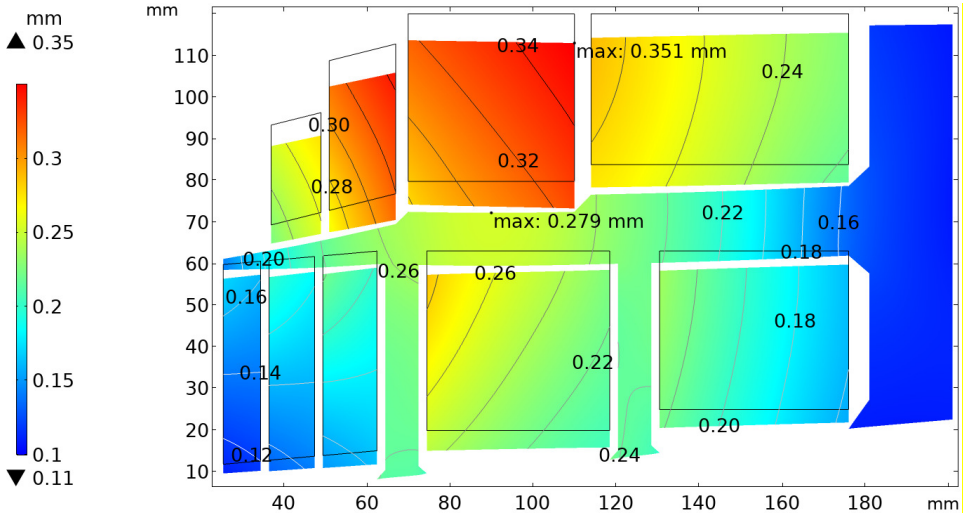

Fig. 14. Axial displacements δ_z at mid-span between pie wedges, magnified twenty-fold. The maximum δ_z is 0.28 mm in the platen and 0.35 mm in the coils.

May contain trade secrets or commercial or financial information that is privileged or confidential and exempt from public disclosure. Such proprietary information is highlighted.

Figure 15 plots the von Mises stress in the coils and support structure. In each of the ReBCO coils the von Mises stress is very nearly 500 MPa, a comfortable margin less than the 600 MPa maximum recommended for the conductor.

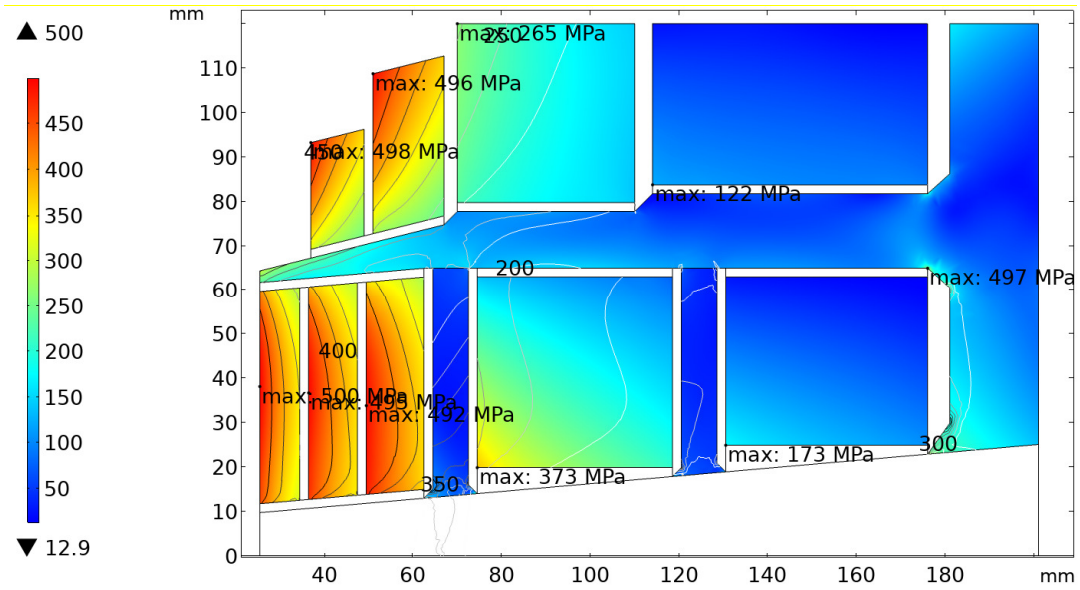

Fig. 15. Von Mises stress, σ_{vM}. At the mid-span between pie wedges, the maximum σ_{vM} is 497 MPa in the platen, 173 MPa in the NbTi coil, and ranges from 122 MPa to 373 MPa in the Nb_3Sn coils and 492 MPa to 500 MPa in the ReBCO coils.

Figure 16 plots the first principal strain in the coils. In the ReBCO coils, it never exceeds 0.387%, a margin of 16% to the 0.45% maximum recommended for the conductor. In the NbTi coil, the maximum strain is only 0.156%; in the Nb_3Sn coils the range is from 0.104% to 0.338%. The platen maximum is 0.474%.

May contain trade secrets or commercial or financial information that is privileged or confidential and exempt from public disclosure. Such proprietary information is highlighted.

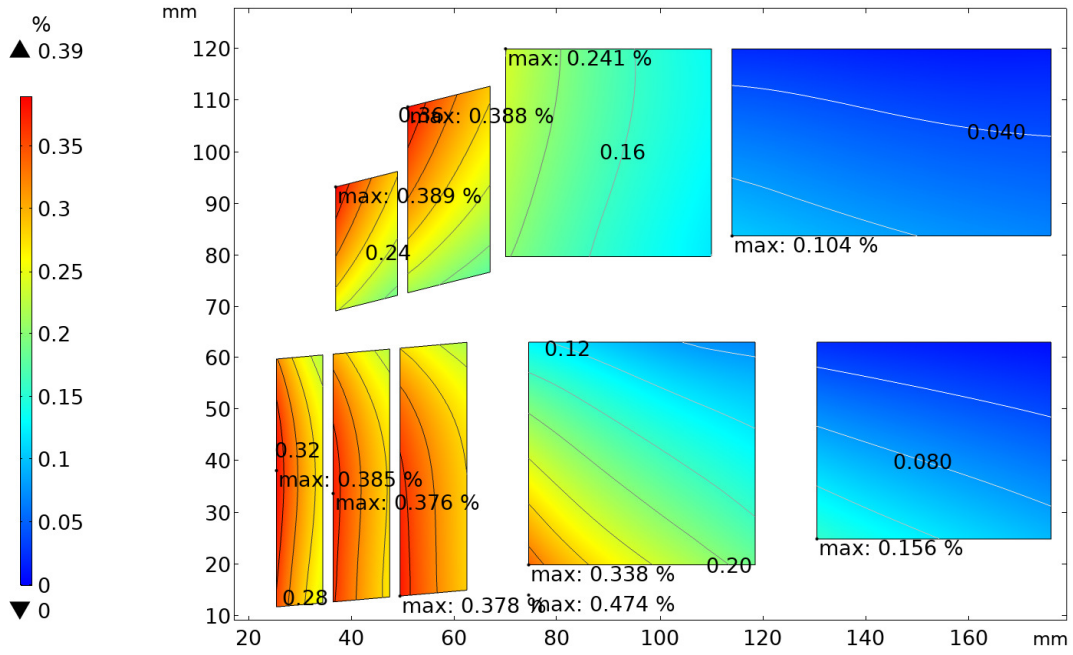

Fig. 16. First principal strain ε_1. At the mid-span between pie wedges, the maximum ε_1 is 0.474% in the platen, 0.156% in the NbTi coil, and ranges from 0.104% to 0.338% in the Nb_3Sn coils and 0.376% to 0.389% in the ReBCO coils.

Figure 17a&b reveals stress concentrations where the support rings bear against the pie wedges. These may be sufficiently localized to be acceptable. If not, gently crowning the pie wedge and/or support rings should spread the load to reduce the stress concentrations.

Table III lists selected parameters of the magnet. The estimated materials cost of magnet is 23% less than the previous design, while simultaneously providing margins on stress and strain.

May contain trade secrets or commercial or financial information that is privileged or confidential and exempt from public disclosure. Such proprietary information is highlighted.

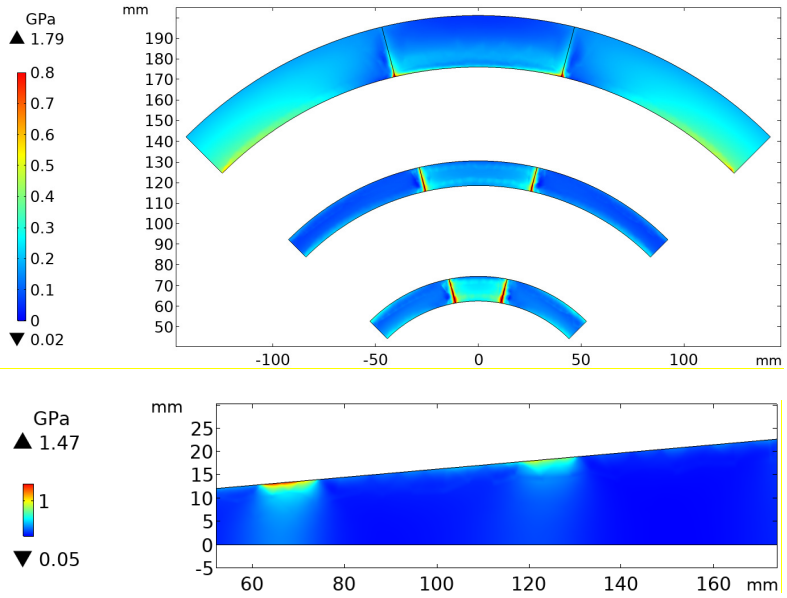

Fig, 17a&b. Localized von Mises stress concentrations where the support rings bear on the pie wedges. Top: Inboard side of support rings. Bottom: Typical radial/axial face of pie wedge.

Table III: Parameters of Illustrative Magnet with Intercoil Platen Support from Below

Intercoil platen supported from below

Parameter	units	Spec	Magnet	Y #1	Y #2	Y #3	Sn #1	NbTi	Y #4	Y #5	Sn #2	Sn #3	Structure
Minimum bore	mm	40.0	51.0										
Minimum split	mm	17.0	19.5										
Min. midplane taper angle	degrees	±5.0	±5.0										
Axial taper angle	degrees		±17.2										
Current density	T		525	525	470	480	250	300	450	430	250	299.9	
Central field	%	25.0	25.00	3.08	3.40	3.87	4.77	3.78	0.38	0.84	1.70	3.18	
$\Delta B/B_0$ @ r = z = 7.5 mm	T	1.40	1.39										
Maximum ambient field	MJ		29.18	29.18	23.5	18.8	13.93	6.97	22.7	18.8	13.87	10.00	
Magnetic energy	kJ		1294										
Max. r j B hoop stress	MPa		446	421	415	446	259	274	394	398	231	273	
Bonded-coil von Mises stress	MPa		500	500	495	492	373	173	498	496	265	122	497
Bonded-coil hoop strain	%		0.389	0.385	0.376	0.378	0.338	0.156	0.389	0.388	0.241	0.104	
Upward Lorentz force, F_z	kN		-3315	0.04	4.1	9.5	24.1	0.8	-86	-309	-869	-2090	
Intercoil-platen design: Cost ratio is 3378 / 4365			=	77.4%		1463		3336			8215		10463
Material				YBCO	YBCO	YBCO	Nb_3Sn	NbTi	YBCO	YBCO	Nb_3Sn	Nb_3Sn	Steel
Conductor requirement	cm^3			162.9	278.7	439.1	2300	3336	155.7	427.2	1821	4094	10463
Normalized unit cost of conductor	- -; %			1	1	1	0	0.05	1	1	0.2	0.2	0.01
Normalized material cost	%		3378	162.9	278.7	439.1	459.9	166.8	155.7	427.2	364.2	818.8	104.6
Percentage of total cost	T/k$		100.0%	4.82%	8.25%	13.00%	13.62%	4.94%	4.61%	12.65%	10.78%	24.24%	3.10%
$\Delta B_0/\Delta\$$			25.0	63.9	41.3	29.8	35.0	76.5	8.2	6.6	15.7	13.1	

May contain trade secrets or commercial or financial information that is privileged or confidential and exempt from public disclosure. Such proprietary information is highlighted.

Design with Magnetic Support of Inboard Coils, Intercoil Platen Support from Above

Figure 18 plots the field magnitude in a magnet of the geometry of Figs. 3c/4c, in which support of the outboard coils is from a robust cantilever supported by a comparably robust ring radially outside the coils. The maximum ambient field coincidentally is the same 28.2 T as in Fig. 10.

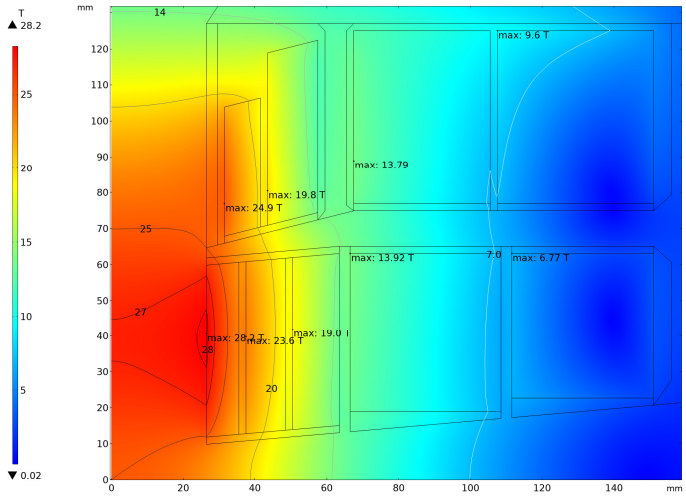

Fig. 18. Field magnitude B for the magnet of Figs. 3c/4c. B_{max} in the ReBCO tape is 28.2 T; selected contours suggest where Nb_3Sn or NbTi suffices instead of HTS: 14 T for Nb_3Sn and 7 T for NbTi. The magnetic energy, U_m, is 1.10 MJ.

Figure 19a&b plots the field homogeneity and fringe field of the magnet of Fig. 18.

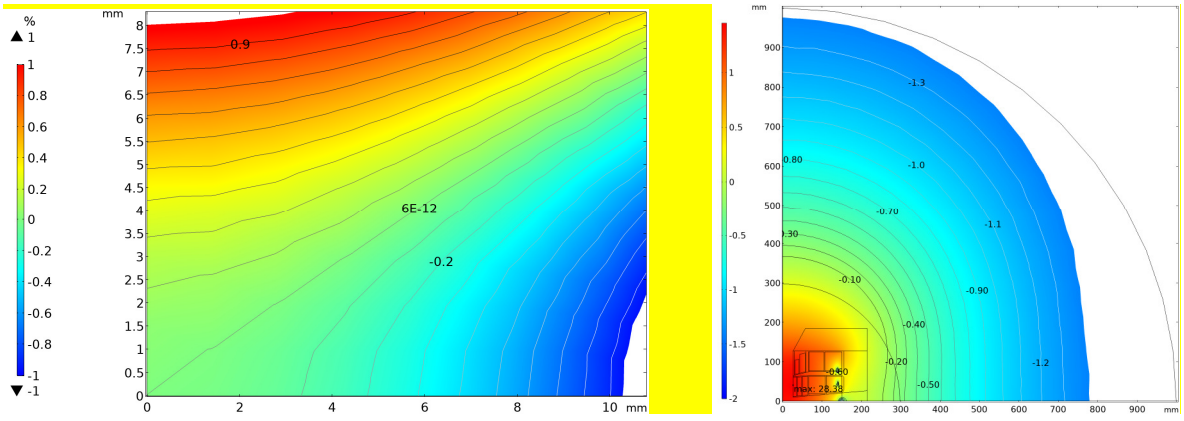

Fig. 19a&b. Field homogeneity and fringe field. Left: The field homogeneity is 1.33% over a cylinder of 7.5 mm radius and half-length. Right: log10|B[kG]|. The successive tesla contours are [$10^{-1.3}$=0.05, 0.064, 0.08, 0.10, 0.125, 0.16, 0.20, 0.25, 0.32, 0.40, 0.50, 0.64, 0.80, 1.0]. On-axis the blue-to-white border ($10^{-1.4} \approx 0.04$ T) nearly reaches the black arc, r = 1 m; extrapolating $B \sim r^{-3}$ predicts a field approximately one twentieth the allowed 0.1 kG at 2 m.

May contain trade secrets or commercial or financial information that is privileged or confidential and exempt from public disclosure. Such proprietary information is highlighted.

Figure 20 plots $|F_z|$, the absolute value of the density of the axial component of Lorentz force. The net upward force, in kN, on each of the five successive inboard coils is 12, 22, 28, 73 and 109; the downward forces on each of the four successive outboard coils is 92, 369, 957 and 1698, a net downward force of 2871 kN.

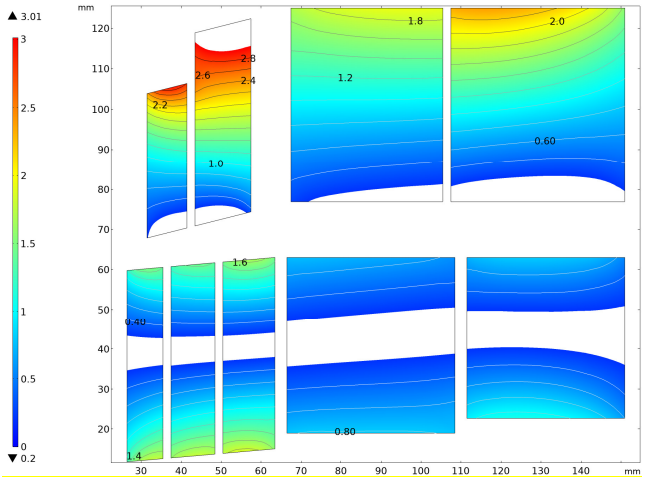

Fig. 20. Absolute value of density of axial Lorentz force in magnet of Fig. 18. Magnetic attraction from outboard coils attracts inboard coils upward, overpowering the downward attraction from coils on the opposite side of the midplane. Within the white band, $|F_z| < 0.2$ N/mm^3. Axially outboard of the band F_z is toward the magnet midplane; axially inboard, it is away from the midplane. The net force on each inboard coil is away from the midplane.

Figure 21a&b plots the axial displacement with a support structure with a Young's modulus of 208 GPa, typical of stainless steel. With a support structure this massive, its maximum axial displacement is a mere 0.44 mm; that in the conductor is very little more: 0.53 mm.

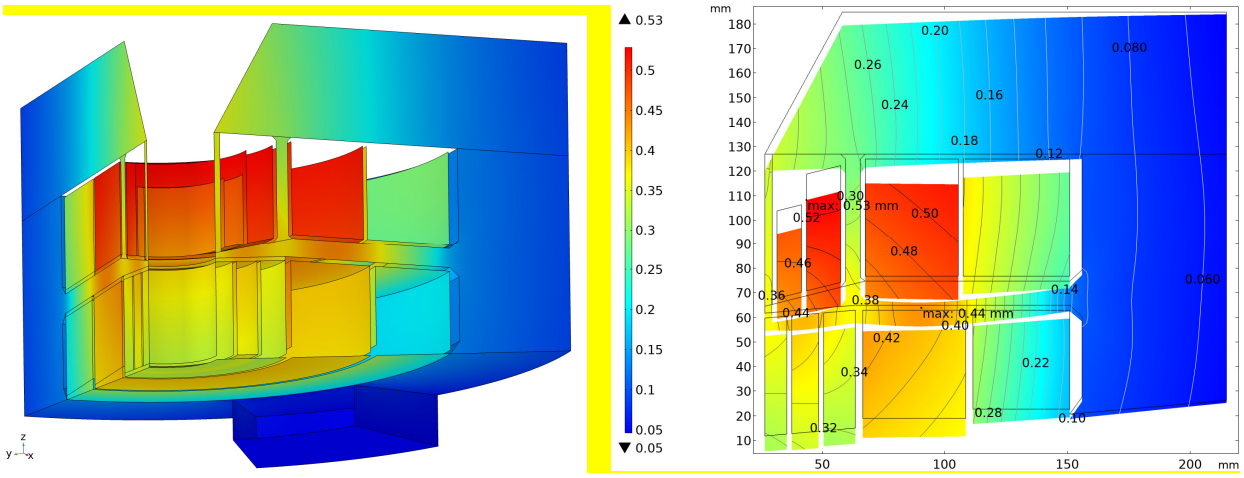

Fig. 21a&b. Axial displacements δ_z , magnified twenty-fold. Left: 3-D. Right: At mid-span between pie wedges. The maximum δ_z is 0.53 mm in the coils and 0.44 mm in the intra-coil platen.

May contain trade secrets or commercial or financial information that is privileged or confidential and exempt from public disclosure. Such proprietary information is highlighted.

Figure 22 plots the von Mises stress. In all five ReBCO coils, it is just shy of 500 MPa, providing a 20% margin to the 600 MPa maximum recommended for the conductor. The more than 1 GPa stress concentration at corners between the platen and rings likely is so localized as to be acceptable.

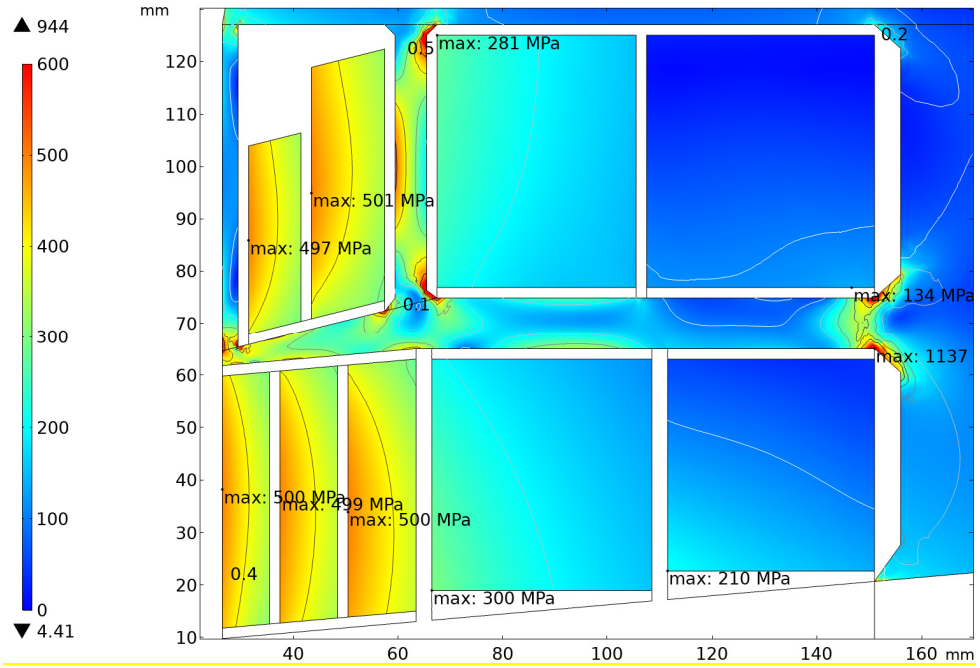

Fig. 22. Von Mises stress, σ_{vM}. In all five of the ReBCO coils the maximum von Mises stress is very nearly 500 MPa; in the NbTi it is 210 MPa; in the Nb_3Sn, it ranges from 134 MPa to 300 MPa. In the platen, it reaches as much as 1.14GPa, but over so small a region as probably to be acceptable.

May contain trade secrets or commercial or financial information that is privileged or confidential and exempt from public disclosure. Such proprietary information is highlighted.

Figure 23 plots the first principal strain, ε_1. In each ReBCO coil, ε_1 is approximately 0.38 %, providing a nearly 20% margin to the 0.45% maximum recommended for ReBCO.

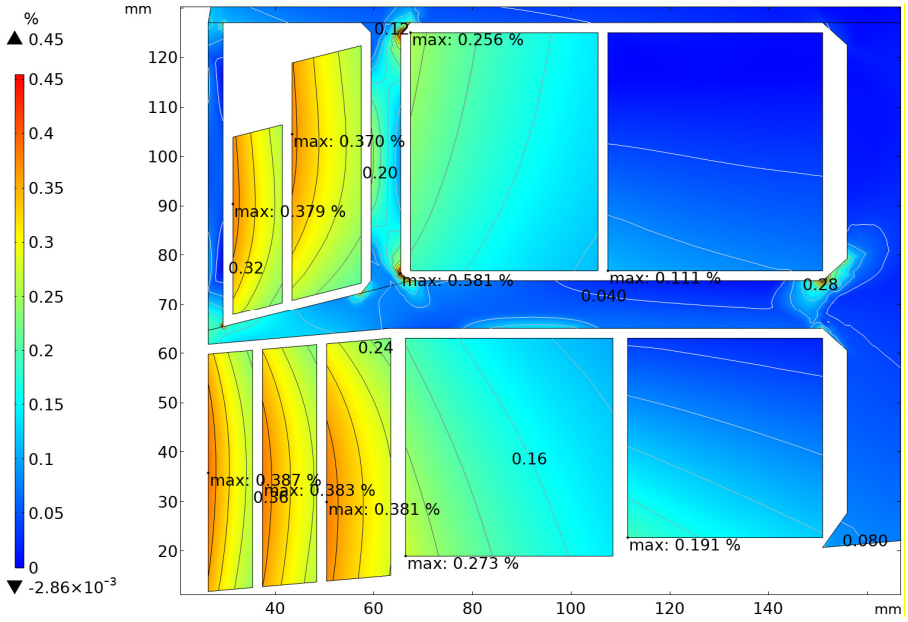

Fig. 23. First principal strain ε_1. In all five ReBCO coils the maximum ε_1 is less than 0.4%; in the NbTi coil it is 0.191%; in the Nb_3Sn coils it ranges from 0.111% to 0.273%. In the platen, it reaches as much as 0.581%, but over so small a region as probably to be acceptable.

Figure 24 plots the von Mises stress concentrations where the pie wedge supports the outermost ring; the maximum reaches only 0.79 GPa in the ring and 644 MPa in the pie wedge.

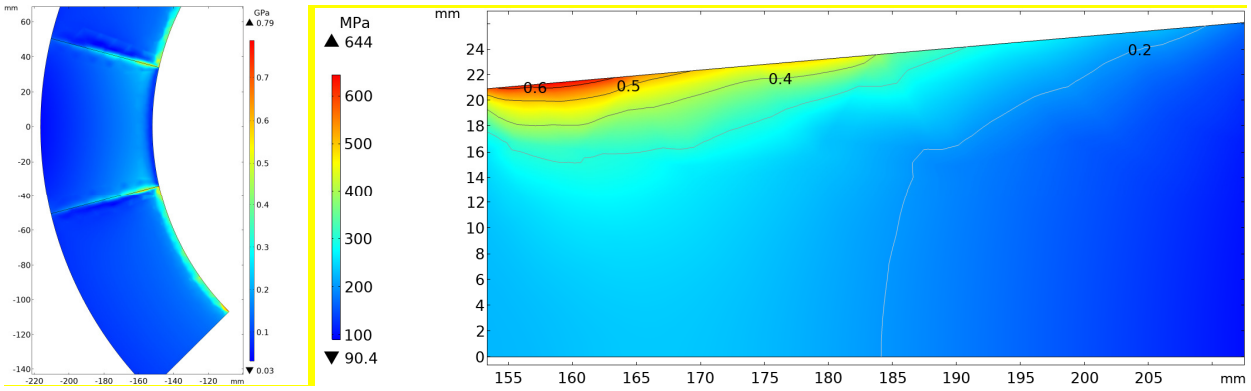

Fig, 24a&b. Localized von Mises stress concentrations where the support rings bear on the pie wedges. Left: Top of pie wedge. Right: Circumferential face of pie wedge.

May contain trade secrets or commercial or financial information that is privileged or confidential and exempt from public disclosure. Such proprietary information is highlighted.

Table IV lists selected parameters of the magnet. The estimated materials cost of magnet coincidentally is almost identical to that of the previous design, which is 23% less than in design 3a/4a. For this design, the margins on stress and strain and strain are even greater than in the previous design, suggesting that the estimated superiority in cost may be even greater than 23%. Furthermore, the design likely will allow a viewing port considerably greater than ±30°.

Table IV: Parameters of Illustrative Magnet with Intercoil Platen Support from Above

Intercoil platen supported from above													
Parameter	units	Spec	Magnet	Y #1	Y #2	Y #3	Sn #1	NbTi	Y #4	Y #5	Sn #2	Sn #3	Structure
Minimum bore	mm	40.0	53.0										
Minimum split	mm	17.0	19.6										
Min. midplane taper angle	degrees	±5.0	±5.0										
Axial taper angle	degrees		±9.0										
Current density	T		510	510	455	462	250	300	510	505	250	300	
Central field	T	25.0	25.02	3.02	3.29	3.72	4.92	3.92	0.39	0.90	1.86	3.00	
$\Delta B/B_0$ @ r = z = 7.5 mm	T	1.40	1.33										
Maximum ambient field	MJ		28.23	28.23	23.6	19.0	13.92	6.77	24.9	19.8	13.79	9.6	
Magnetic energy	kJ		1104										
Max. r j B hoop stress	MPa		444	424	416	444	231	224	416	436	231	231	
Bonded-coil von Mises stress	MPa		501	500	499	500	300	210	497	501	281	134	1137
Bonded-coil hoop strain	%		0.387	0.387	0.383	0.381	0.273	0.191	0.379	0.370	0.256	0.111	0.581
Upward Lorentz force, F_z	kN		-2871	12	22	28	73	109	-92	-369	-957	-1698	
Cantilever open-midplane design: Cost ratio is			=	77.4%		1492		2628			7423		27059
Material				YBCO	YBCO	YBCO	Nb_3Sn	NbTi	YBCO	YBCO	Nb_3Sn	Nb_3Sn	Steel
Conductor requirement	cm^3			168.3	285.3	447.0	2035	2628	165.1	426.5	1988	3400	27059
Normalized unit cost of conductor	- -; %			1	1	1	0.2	0.05	1	1	0.2	0.2	0.01
Normalized material cost	%		3379	168.3	285.3	447.0	407.0	131.4	165.1	426.5	397.5	680.0	270.6
Percentage of total cost	T/k$		100.0%	4.98%	8.44%	13.23%	12.05%	3.89%	4.89%	12.62%	11.77%	20.13%	8.01%
$\Delta B_0/\Delta\$$			25.0	60.5	39.0	28.1	40.8	100.8	7.9	7.1	15.8	14.9	

Winding and 77 K Testing of HTS Conical Coil

Conical coils of broad, thin tape were wound utilizing, for economy, stainless steel to develop the winding techniques, and then ReBCO tape, 12 mm wide, available from previous projects. Conicality can significantly improve the efficiency of magnets with midplane viewing ports that flare axially with distance from the magnet axis. The coil cross section is ideal—not rectangular, but a parallelogram whose inboard edge parallels the flare angle of the port. The conductor is wound into pancakes that are dished slightly, forming a very blunt cone, like a nearly-flat cone spring.

Figure 25a shows the winding mandrel that imparts the conical shape to the coil. Figure 25b shows four views of a practice coil wound with stainless steel tape of identical width and similar thickness to the actual HTS tape.

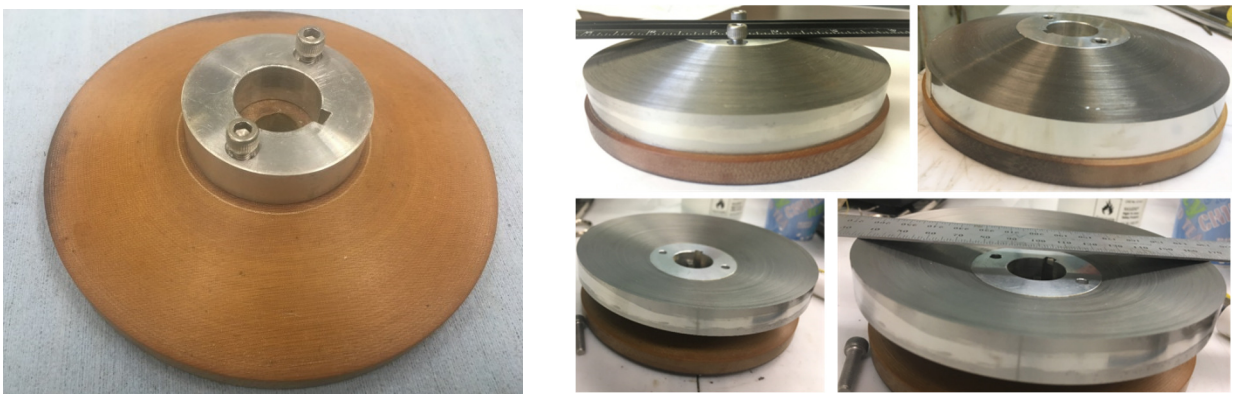

Fig. 25a&b. Left: Mandrel for winding conical coil. Right: Four views of a practice winding of a conical coil with I.D. = 51 mm, O.D. = 127 mm, cone angle = 15°, and conicality = 10.2 mm.

Figure 26a shows the winding of a conical coil on the mandrel shown in Fig. 25a; the coil has several voltage taps installed for diagnostics and testing. Figure 26b shows the fully wound 315-turn coil: inner diameter = 51 mm, outer diameter = 127 mm, cone angle = 15°, and conicality = 10.2 mm. The conductor is 88 meters of ReBCO tape 12 mm wide by 0.12 mm thick.

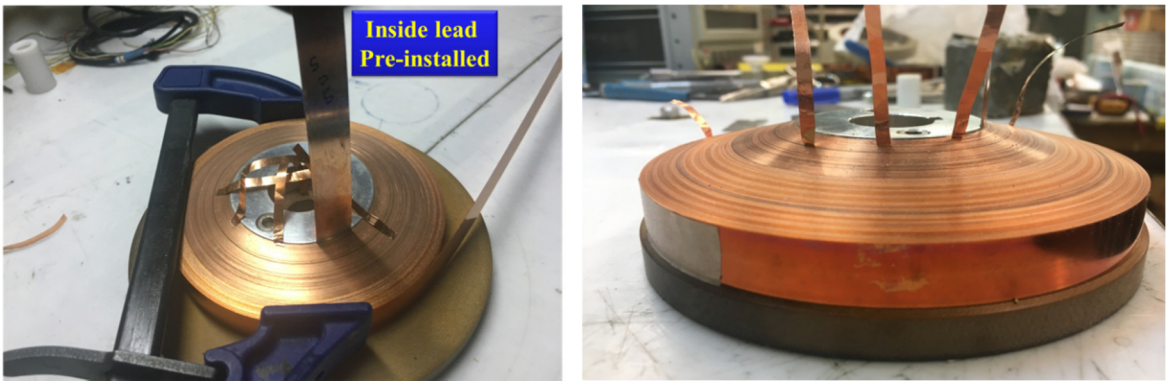

Fig. 26a&b. HTS coil on its conical mandrel. Left: During the winding process; inside lead and voltage-taps pre-installed. Right: Winding completed.

Figure 27 shows the fully wound conical coil, with the voltage taps now folded down. The straightedge in Fig. 27b helps to reveal the 10.2-mm magnitude of conicality.

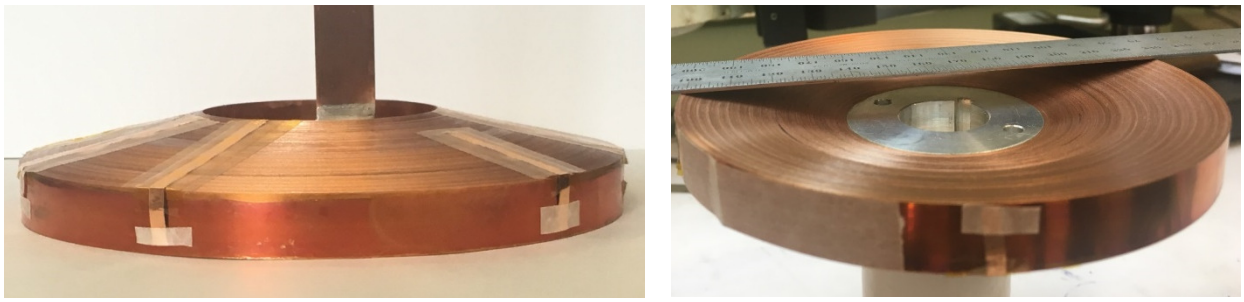

Fig. 27a&b. Conical coil of 51 mm I.D., 127 mm O.D., 15° cone angle, and 10.2 mm conicality; conductor is 88 m (315 turns) of ReBCO tape 12 mm wide by 0.12 mm thick. Left: View from crowned side. Right: View from dished side.

Operation of the coil involved testing with four stages of inner diameter, tabulated in the first row of Table V, as inner turns were removed to track down and eliminate conductor that failed to become superconducting.

Table V: Parameters of the conical no-insulation HTS coil.

Parameters of the PBL/BNL HTS conical coil for Neutron scattering					
		Test #1	Test #2	Test #3	Test #4
Coil inner diameter	mm	50.8	74.970	81.504	83.924
Coil thickness	mm	38.1	26.015	22.748	21.538
Cone angle	degree	15	15	15	15
Tape width	mm	12.05	12.05	12.05	12.05
Nominal tape thickness	mm	0.121	0.121	0.121	0.121
Number of turns		315	215	188	178
Coil outer diameter	mm	127	127	127	127
Vertical drop	mm	10.21	6.97	6.10	5.77
Conductor length	meter	88	68	62	59

Figure 28 shows the conical coil in preparation for Test #1; Fig. 28b shows the internal voltage tap of copper strips connected to external wiring.

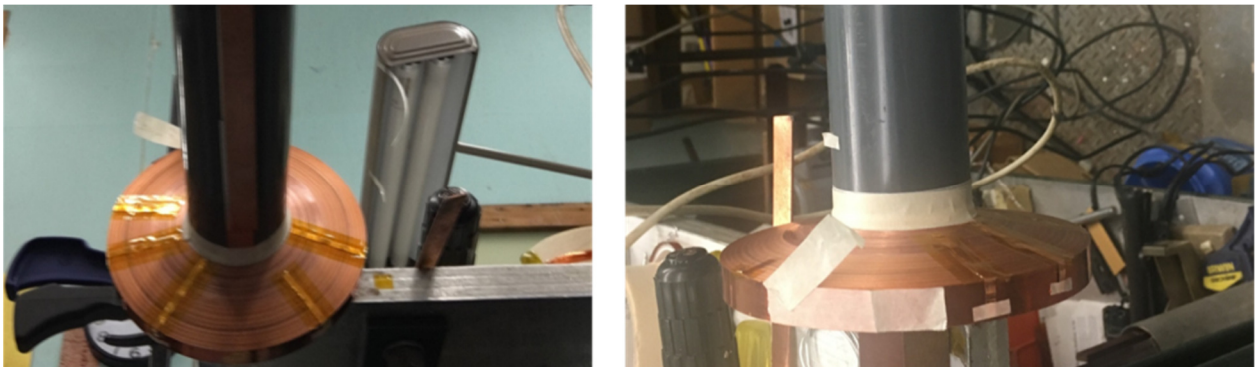

Fig. 28a&b. Conical coil of ReBCO tape during preparations for the first test in liquid nitrogen.

Figure 29a shows, for Test #1, V(I) curves for the entire coil and for six subsections, bordered by turns 0, 10, 25, 50, 100, 300 and 315. The coil carried 130 A, the maximum expected of it, so the conical winding was successful. However, whereas other subsections were superconducting until at least ~110 A, subsection 100-300 was resistive from the get-go. Figure 28b is a histogram of the voltage fraction in each coil subsection (blue) and voltage per unit length (red) when the voltage across the entire coil is 8.8 mV, an average voltage gradient of 0.1 μV/cm.

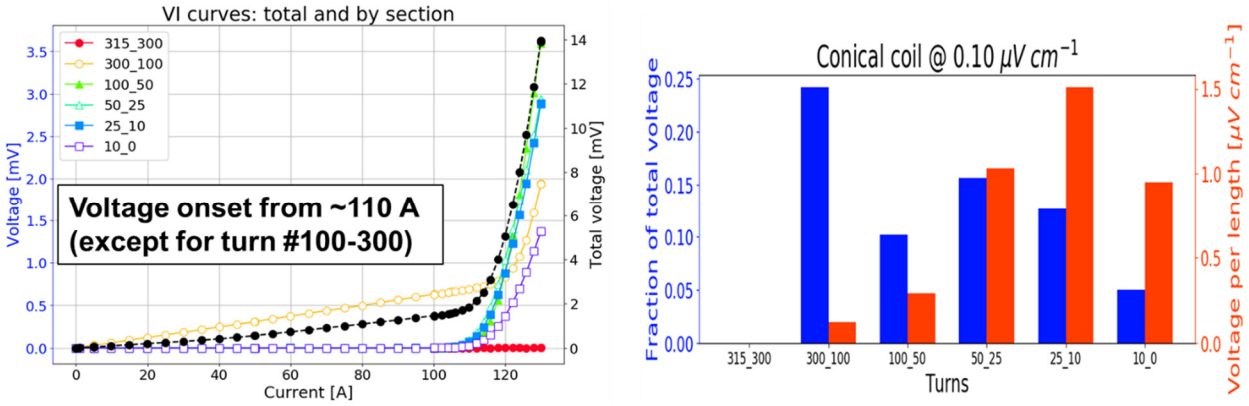

Fig. 29. Left: V(I) for six magnet subsections, bordered by turns 0, 10, 25, 50, 100, 300 and 315. Right: Voltage fraction in each coil subsection (blue), and voltage gradient dV/ds (red) when the total coil voltage is 8.8 mV, an average voltage gradient of 0.1 μV/cm. The conical coil reached the full current expected of it.

Figure 30a reveals that the proportionality of voltage and current in coil subsection "100-300" implies a resistance of 6.14 μΩ; such a resistance could be caused by superconductor that locally is grossly defective or missing entirely. That the coil could be tested to full current is because the absence of insulation permits current to bypass into neighboring turns.

To localize the defect, more voltage-taps were installed between turn #100 and #300, as pictured in Figures 30b&c.

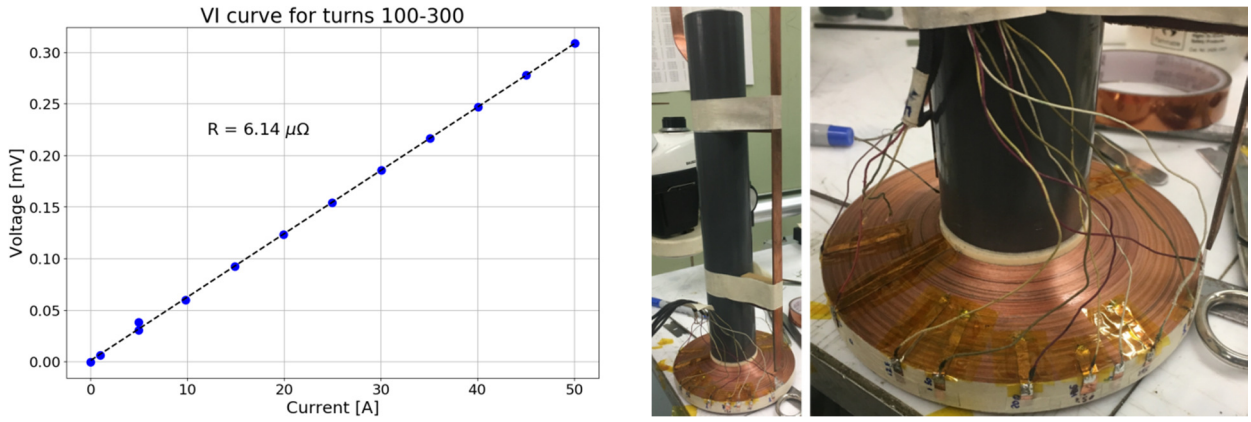

Fig. 30a-c. Left: V(I) in coil subsection "100-300". Center & right: Coil prepared for Test #2, with inner 100 turns removed and voltage taps added to locate the source of resistance in coil subsection "100-300".

Figure 31a reveals, from Test #2, that the source of resistance is between turns #100 and #150, prompting Test 3, with another 27 turns removed from the coil. However, neither Test #2, nor Test #3, nor physical examination of the removed conductor detected any conductor defect.

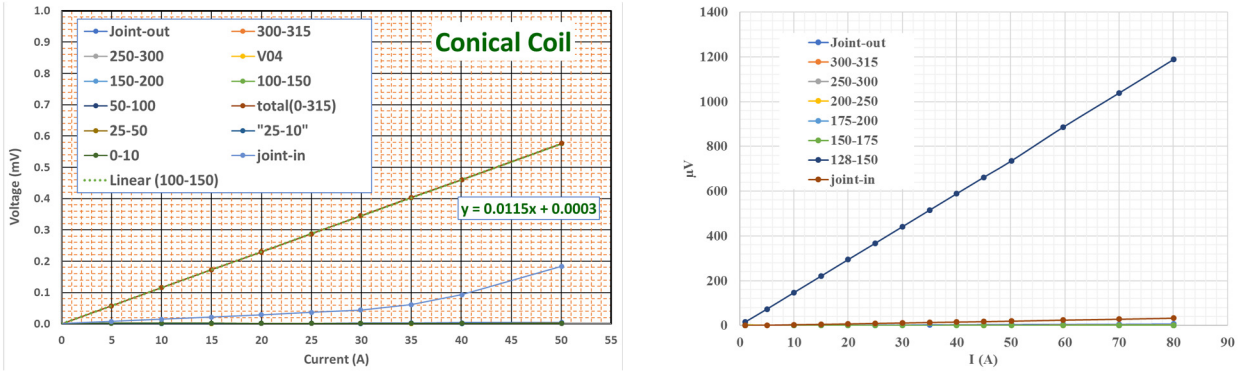

Fig. 31a&b. V(I) of Tests #2 and #3, with turns removed and more voltage taps installed to localize the source of resistance. The resistance is between turns #100 and #150 (Left), and (Right), turns #128 and #150.

Removal of ten more turns (total 137 turns removed) from the inside of the coil uncovered a lap joint; Test #4 confirmed, as in Fig. 32, that the coil at last was devoid of early-onset voltage, evincing superconductivity until a current of nearly 130 A; current-sharing extended the range of operation to 150 A. In Test #4 the conical coil performed to full expectations, confirming the success of conical winding.

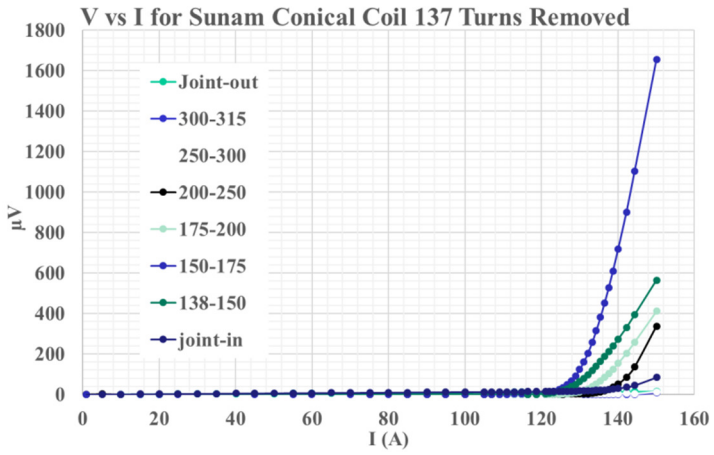

Fig. 32. V(I) in Test #4, with 137 turns removed; the resistive section has been removed, so that the whole coil now remains superconducting until nearly 130 A.

Testing of the ReBCO coil, at 77 K, confirmed its tolerance to localized internal resistance and to the handling associated with installation of additional diagnostic voltage taps to uncover and remove this local resistance. Even before removal of the multi-centimeter region of high resistance, the coil was able to operate to nearly full current, because the no-insulation winding allowed current to bypass the defect. The higher current in test #4 was primarily due to the fact the coil in test number #4 had a fewer turns, larger inner diameter and hence a lower maximum field on the conductor than the coil in test #1.

References

1. Nat. Res. Council, "High Magnetic Field Science and Its Application in the United States: Current Status and Future Directions," Washington, DC, Nat. Acad. Press. https://www.nap.edu/read/18355, ISBN 0309387787, 9780309387781 (2013) doi: https://doi.org/10.17226/18355.
2. Workshop on Probing Matter with X-Rays and Neutrons at the National High Magnetic Field Laboratory, Tallahassee, FL, May 10-12, 2005.
3. B. Winn, M.B. Stone, et al., Workshop on Neutron Scattering and High Mag. Fields, Sept. 4-5, 2013, https://neutrons.ornl.gov/sites/default/files/WorkshopReportFINAL_FINAL.pdf. ORNL/TM-2014/652, doi: 10.2172/1410956 (2014).
4. B. Winn, et al. Tech. Report: Ultra-High Field Magnets for X-Ray and Neutron Scattering using High Temperature Superconductors, https://info.ornl.gov/sites/publications/Files/Pub71968.pdf. ORNL/TM-2016/712, DOI: 10.2172/1432171 (2017).
5. O. Prokhnenko, et al. Time-of-flight Extreme Environment Diffractometer at the Helmholtz-Zentrum Berlin. Rev. Sci. Instr. **86**, 033102 (2015); doi: 10.1063/1.4913656.
6. HFM/EXED. High Magnetic Field Facility for Neutron Scattering. https://www.helmholtz-berlin.de/pubbin/igama_output?modus=einzel&gid=1939&sprache=en.
7. F.J. Brown, J. Phys.: Conf. Ser. **251**, 012093 (2010).
8. R.B.E. Down, et al., J. Phys.: Conf. Ser. **251** 012092 (2010).
9. O. Kirichek, et al., J. Phys.: Conf. Ser. **400** 052013 (2012).
10. A.T. Holmes, et al., Rev. Sci. Instr. **83**, 023904 (2012); doi: 10.1063/1.3688657.
11. T. Panesor & E. Woodfield, "Neutron scattering," Institute of Physics 2010, https://www.iop.org/publications/iop/2011/file_47455.pdf
12. R. Gupta, et al., "Open-Midplane Dipole Design for LHC IR Upgrade," MT18, Morioka City, Japan (2003).
13. R. Gupta, et al., "Optimization of Open Midplane Dipole Design for LHC IR Upgrade," PAC'05, Knoxville, TN, USA (2005).
14. R. Weggel, et al., "Open-Midplane Dipoles for a Muon Collider," PAC11, NY, NY (2011); BNL-95145-2011-CP.
15. R. Gupta, et al., "High Field HTS R&D Solenoid for Muon Collider," presented at 2010 Applied Superconductivity Conf., Trans. on Appl. Supercond.
16. R. Weggel, et al., "An ongoing study to test a YBCO HTS magnet at fields approaching 40 T," Neutron Factory and Muon Collider Collaboration-DOC-553, 2010.
17. Y. Shiroyanagi, R. Gupta, P. Joshi, H. Kirk, R. Palmer, W. Sampson, P. Wanderer, D. Cline, A. Garren, J. Kolonko R. Scanlan, R. Weggel, "15+ T HTS Solenoid for Muon Accelerator Program," 3rd Int. Particle Acc. Conf. (IPAC 2012).